energies

MDPI

Article

Energetic and Exergetic Analyses of an Experimental Earth–Air Heat Exchanger in the Northeast of France

Wael Zeitoun [1,2], Jian Lin [1] and Monica Siroux [2,*]

[1] ICUBE, IUT Robert Schuman, University of Strasbourg, 67400 Illkirch-Graffenstaden, France
[2] INSA Strasbourg ICUBE, University of Strasbourg, 67000 Strasbourg, France
* Correspondence: monica.siroux@insa-strasbourg.fr; Tel.: +33-388144753

Abstract: Earth–air heat exchanger (EAHE) systems are used to pre-heat or pre-cool air before entering into a building using shallow geothermal energy. Assessment of EAHE systems is important to quantify the profitability of these systems. For this purpose, an EAHE system built at ICUBE at the University of Strasbourg in the northeast of France was studied using energy and exergy analyses for a typical heating period (between 25 February and 3 March). Energy analysis was used to determine the heat gained by the air in the system during the studied period and to determine the Coefficient Of Performance (*COP*) of the system. Additionally, exergy analysis, which considered temperature, pressure, humidity, and the variation in the control volume boundary temperature, was realized to determine inefficiencies in the system by determining the exergy destroyed in each component of the system and evaluating its exergetic efficiency. Results showed that the heat energy gained using the system was around 63 kWh and that the exergetic efficiency of the system was about 57% on average. The comparison of exergetic efficiency between the EAHE components showed that the fan has the lowest performance and should be improved to achieve better overall performance.

Keywords: earth–air heat exchanger; horizontal ground heat exchanger; energy analysis; exergy analysis; shallow geothermal energy; renewable energy

check for updates

Citation: Zeitoun, W.; Lin, J.; Siroux, M. Energetic and Exergetic Analyses of an Experimental Earth–Air Heat Exchanger in the Northeast of France. *Energies* **2023**, *16*, 1542. https://doi.org/10.3390/en16031542

Academic Editors: Ákos Lakatos and Gianpiero Colangelo

Received: 15 December 2022
Revised: 17 January 2023
Accepted: 28 January 2023
Published: 3 February 2023

Copyright: © 2023 by the authors. Licensee MDPI, Basel, Switzerland. This article is an open access article distributed under the terms and conditions of the Creative Commons Attribution (CC BY) license (https://creativecommons.org/licenses/by/4.0/).

1. Introduction

Buildings are the largest energy-consuming sector in the world, accounting for over one-third of total final energy consumption, the majority of which is consumed for space heating and cooling, along with water heating, which are estimated to account for nearly 60% of global energy consumption in buildings [1]. This share increases to about 79% in the European Union (EU) for space and water heating only (Odyssee database as cited in [2]). On current trends, energy needs for space cooling, almost entirely as electricity, will more than triple between 2016 and 2050, driven mainly by the residential sector [3].

According to the British Petroleum (bp) Statistical Review of World Energy in 2021, more than 84% of the world's primary energy consumption is still generated from fossil fuels (oil, natural gas, and coal) [4]. This generation of energy is accompanied by high CO_2 emissions affecting the global warming of the Earth. If no action is taken to improve energy efficiency in the buildings sector, energy demand is expected to rise by 50% by 2050 [1], which could increase the use of fossil fuels and, thus, CO_2 emissions.

During the 2015 United Nations Climate Change Conference in Paris, parties agreed to limit global warming to well below 2 °C and pursue efforts to limit it to 1.5 °C as a global framework to avoid dangerous climate change. Achieving this goal requires an estimated 77% reduction in total CO_2 emissions in the buildings sector by 2050 compared to levels in 2013 [1]. The reduction in CO_2 emissions can be achieved by reducing energy demands and by increasing the use of renewable clean energy sources. The use of renewable energy is still low compared to the use of unclean energy; for example, in the EU, renewables currently provide only 23% of energy consumption in the heating and cooling sector [5].

The temperature distribution inside the Earth can provide clean, renewable energy in the form of geothermal energy. While the underground temperature near the surface is affected by the ambient weather, the temperature then increases deeper into the Earth, mainly due to radioactive elements that decay and release heat. Following this temperature distribution, two types of systems are used to extract this heat: high enthalpy systems (>150 °C) and low enthalpy systems. High enthalpy systems extract heat at temperatures that can reach an order of 200–300 °C sufficient for electricity generation. This temperature could be reached by drilling only a few hundred meters near plate boundaries or volcanoes; however, within the plates, it could need drilling by up to 5 km. On the other hand, low enthalpy systems are installed in shallow underground layers ranging from a couple of meters up to 400 m deep, depending on the capacity and technology of the system. Low enthalpy systems work on low temperatures from below 150 °C down to near ambient temperature. On average, the underground temperature at 10 m depth remains constant throughout the year and substantially equals the average ambient temperature above ground [6]. Above this depth, near the surface, the temperature in the winter (or during the night) is usually higher than the ambient air temperature, and in the summer (or during the day), it is lower. This behavior of the temperature field is consistent with heating and cooling periods of buildings, where heat can be extracted or released to the rooms from the underground soil, depending on the season. One method to benefit from this behavior of the shallow underground temperature field is the earth–air heat exchanger (EAHE).

The EAHE is a simple pipe buried under the ground at very shallow depths that usually do not exceed 10 m. It is not to be confused with a ground-source heat pump (GSHP) where, in EAHE, air is the heating transfer fluid. Air passes in the pipe from one end, it becomes heated or cooled by the surrounding soil, and then it is either used directly in the building or passes through additional systems (e.g., an HVAC system). Mechanical devices (such as fans) are usually used to circulate the air, or passive methods are used to create adequate pressure difference. In this manner, the EAHE reduces the energy consumption in buildings from nonrenewable sources and decreases CO_2 emissions.

As with all energetic systems involving heat and mass transfer, energy analysis of the EAHE is necessary to assess the performance of the system under certain conditions. This analysis allows the sizing of the system according to the needs and surrounding conditions. Additionally, energy analysis helps to identify different parameters affecting the performance of the system and to quantify them. In the case of EAHE, many parameters affect the system, especially the surrounding environment, such as the underground temperature field, thermophysical properties of the soil and the pipe, moisture content around the pipe, all the characteristics and properties of the flow, and the outside climatic conditions.

Energy analysis is based on the first law of thermodynamics—energy balance; however, the second law also governs the behavior of the system. The second law studies the entropy balance and quantifies entropy generation resulting from irreversible processes in the system. By this, the second law can determine how much of the heat can be converted into work and evaluate the energy lost due to irreversible processes; combining it with the first law results in a new balance called exergy balance.

Exergy is defined as the maximum amount of work that can be produced by a stream or system as it is brought into equilibrium with a reference environment, and it is a measure of the available energy (available to do work). Alternatively, exergy is the minimum theoretical shaft work or electrical work required to form a quantity of matter from substances present in the environment and bring the matter to a specified state [7]. Exergy analysis is used to analyze the performance of the system at the reversible limit and to estimate the departure from this limit. The departure from the reversible limit is due to irreversible processes. The sources of these irreversible processes can be identified by applying the exergy analysis separately to each component of the system, thus detecting the inefficiencies of the system. Outputs of the exergy analysis can be used for the improvement of systems in terms of efficient energy use. The efficiency of the system calculated on the basis of exergy terms provides a more realistic assessment of the capabilities of the system than using normal energy efficiency.

Although the EAHE is not a system that produces work, analyzing it in terms of exergy provides a better assessment of the system and helps to improve its efficiency after identifying the sources of exergy destruction. The literature contains many articles studying exergy analysis of thermal systems but few on shallow geothermal systems such as GSHP and EAHE. Esen et al. [8] investigated the energetic and exergetic efficiencies of the GSHP system as a function of depth trenches for the heating season using two horizontal exchangers buried at different depths with a water–antifreeze solution as the heat transfer fluid. Yildiz et al. [9] studied the exergetic performance of a solar photovoltaic system (PV) assisted closed-loop EAHE that is used for greenhouse cooling in Turkey. They determined the exergy destruction in the system and the exergetic efficiency, which was found to be 59.6% for the EAHE. Hepbasli [10] presented a study that deals with modeling, analyzing, and assessing the performance of a greenhouse heating system with EAHE in the closed-loop mode. He assessed the EAHE system using both energy and exergy analysis methods from the heat generation to the greenhouse envelope and compared its performance through both energy and exergy efficiencies. Misra et al. [11] evaluated the thermal performance of the EAHE system with dry and wet soil during the peak summer season in India. The second law analysis showed that the maximum exergetic efficiency is 52.25% and 53.18% for dry and wet soil EAHE systems, respectively; however, the effect of pressure variation inside the pipe on the exergetic analysis was not considered. In another paper, Afrand et al. [12] studied two configurations of hybrid solar–EAHE systems under Kermanshah, Iran, weather conditions. They evaluated the energetic and exergetic aspects of both configurations, including an examination of the impacts of different influential parameters of them without considering the effect of pressure variation inside the pipe on the exergetic analysis. Ozgener et al. [13,14] applied the exergy analysis to an EAHE used for greenhouse cooling in Turkey. Exergetic efficiencies of the system components were determined to assess their individual performances, but they considered constant soil temperature along the pipe when calculating the exergy of heat transfer. To the best of the authors' knowledge, none of these studies considered temperature, pressure, humidity, and the control volume boundary temperature variations at the same time.

This study aims at evaluating the performance of an experimental EAHE used for heating/cooling a building. Energy and exergy analyses are applied to determine the efficiency of the system from both perceptions. Exergy analysis also shows the exergy destruction in the components of the EAHE to identify irreversibility sources and for possible enhancement of the system. To achieve more accurate results in this study, the performance of the EAHE was determined using pressure, humidity, and temperature measurements and considering variable control volume boundary temperature when calculating the exergy of heat transfer. Measurements were performed on an experimental EAHE at ICUBE, University of Strasbourg, France. Variable air and wall temperatures were considered along the pipe, as explained in the different sections.

2. Experimental Methodology

2.1. Experimental Setup

The experimental EAHE is located at IUT Robert Schuman, University of Strasbourg, Illkirch, France (48°31′50.1″ N, 7°44′17.4″ E). The system is composed of a polyethylene pipe buried under the ground up to a depth of 1.2 m with a total length of 29 m. The air is circulated in the pipe using a fan installed at the outlet, and at the inlet, an air filter is added to trap dust. The pipe starts vertically down to a certain depth and then continues horizontally with a slope of 2% to gather any water that accumulates and pump it out. At the exit, the pipe has a vertical part again to drive air to the surface. From now on, "pipe" is referred to the horizontal part. The characteristics of the pipe used are given in Table 1.

Table 1. Pipe characteristics.

Parameter	Symbol	Values	Unit
Total length	L_{tot}	29	m
Outer diameter	D_{out}	0.20	m
Inner diameter	D_{in}	0.17	m
Thermal conductivity	λ_{pipe}	0.50	$W{\cdot}m^{-1}{\cdot}K^{-1}$

The horizontal part of the EAHE pipe was divided into three sections where each section was coated by a different type of coating soil: (1) sand; (2) sand–bent, a mix between sand and bentonite (3%); and (3) initial natural earth soil (Figure 1). In all sections, the pipe rests on a layer of stabilizer sand below the coatings, as represented in Figure 2. More details about the study of the effect of using different coating soils can be found in the articles published by Cuny et al. [15–17], as this is not the scope of this paper. Characteristics of the EAHE sections are given in Table 2. Note that the depth is taken at the middle of each section, where it is not constant along the pipe, as explained before.

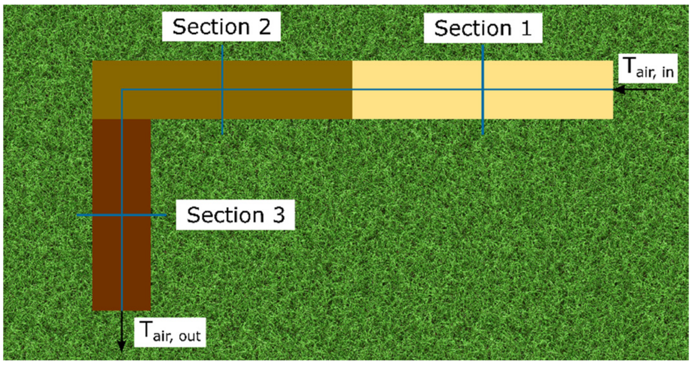

Figure 1. Top-view of the EAHE with section division.

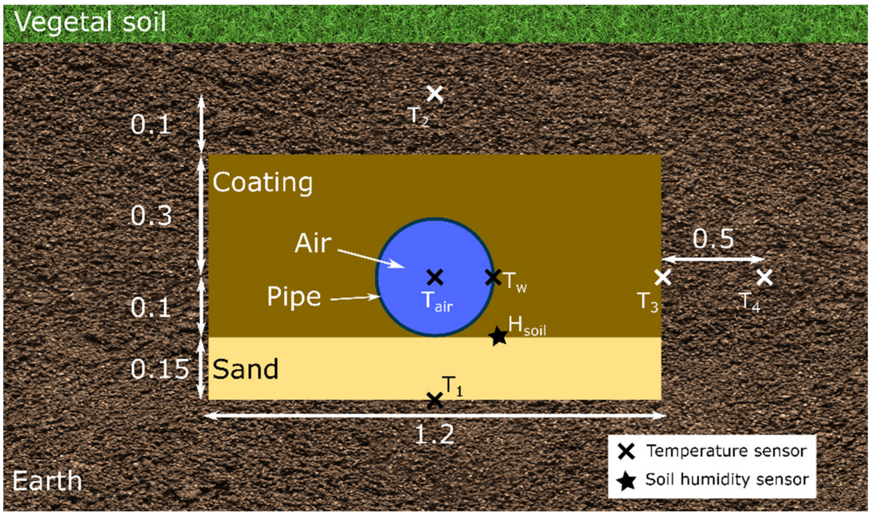

Figure 2. System layers and positions of sensors. All dimensions are in meters.

Table 2. Characteristics of the EAHE sections.

Section	Coating	Depth [1] (m)	Length (m)
1	Sand	0.73 ± 0.02	10.40 ± 0.01
2	Sand–bent	0.92 ± 0.02	10.40 ± 0.01
3	Natural soil	1.2 ± 0.02	8.20 ± 0.01

[1] Depth is considered at the middle of each section.

2.2. Metrology

Each section of the EAHE is associated with a vertical cross-section at its middle in which soil moisture and temperatures at different points are measured. Cross-sections are numbered from 1 to 3, respectively: sand, sand–bent, and natural soil. In each cross-section, seven PT100 sensors measure the temperature with an uncertainty of 0.1 °C. The location of each sensor in the cross-section is represented in the scheme presented in Figure 2. In each section, there is also a soil moisture sensor (TRIME©-pico64) placed at the boundary between the stabilizer sand and the coating, as shown in the scheme. In addition, the temperature and relative humidity of air were measured using an EE061 probe (±3% RH (10–90% RH), ±5% RH (<10% RH and >90% RH)) after the filter at the inlet and before the fan at the outlet of the pipe. The recording of all measurements was performed by a data acquisition system (Keithley 3706A), and data were recorded every 20 min. For the purpose of this paper, only the temperature measurements of the air and wall of the pipe are needed.

Velocity and pressure of air flow were also measured at different locations in the pipe. It is assumed that there is a negligible effect of temperature and humidity on the mechanical characteristics of the flow and that they remain constant in the given configuration. Thus, velocity and pressure measurements were performed once. Testo 435-4 device was used to make the measurements using its fan anemometer (Vane measuring probe 0635 9435) and differential pressure measuring pitot tube (model number: 0635 2145). The pressure was measured at the inlet, then just after the inlet air filter, then before the outlet fan, and at the outlet using small holes in the pipe. The pressure was measured as the difference between the static pressure in the pipe and the atmosphere, then the absolute static pressure at each position was calculated using the ambient atmospheric pressure at the measurement time, which was 102,160 Pa. Measured values of the pressure are shown in Table 3. The velocity was measured by attaching the anemometer with its related funnel tube to the inlet of the pipe and then considering constant mass flow rate and density of air along the funnel, the velocity at the inlet of the pipe was calculated as being $U_{air} = 2.4\ \mathrm{m/s}$ with an uncertainty of $\pm 0.136\ \mathrm{m/s}$. For achieving this velocity, the electric power consumption of the fan was measured to be $\dot{W}_{electric} = 39$ W with an uncertainty of ±2.17 W.

Table 3. Pressure measurements.

Location	Pressure Difference (Pa)	Absolute Pressure (Pa)	Uncertainty
Inlet	−0.07	102,152	±0.02 hPa (0 to + 2 hPa)
After filter	−0.34	102,126	
Before fan	−0.67	102,093	
After fan (Outlet)	−0.08	102,152	

3. Analysis Methodology

3.1. Assumptions

As the system has many parameters and factors affecting its performance, some assumptions were made to reduce the complexity of the mathematical model. Similar assumptions were considered in other studies ([9–14]):

- One-dimensional flow in the control volume;
- Steady-state mass and heat transfer;
- Incompressible fluid flow;
- Constant wall and air temperature in each section;
- Neglection of radiation heat transfer inside the pipe;
- Constant air velocity;
- Uniform air flow along the length of the buried pipes;
- Neglection of heat transfer at the vertical inlet and exit of the pipe;
- Neglection of heat transfer through the filter and the fan;

- Constant humidity ratio through the fan.

3.2. Material Properties

Several air and water vapor properties are used in the calculations. The specific heat capacity $C_{p,a}$ and the density ρ_a of air were calculated using formulas given by Zografos et al. [18]:

$$C_{p,a}(T) = 1.3864 \cdot 10^{-13} \cdot T^4 - 6.4747 \cdot 10^{-10} \cdot T^3 + 1.0234 \cdot 10^{-6} \cdot T^2 \\ -4.3282 \cdot 10^{-4} \cdot T + 1.0613 \quad [\mathrm{kJ}/(\mathrm{kg} \cdot \mathrm{K})] \quad \text{for } 100\ K < T < 3000\ K \tag{1}$$

$$\rho_a(T) = \frac{345.57}{T - 2.6884} \quad [\mathrm{kg}/\mathrm{m}^3] \quad \text{for } 150\ K < T < 3000\ K \tag{2}$$

The saturation pressure of water vapor P_{sat} [Pa] was calculated using the formulas given by Huang [19]:

$$P_{sat}(T) = \begin{cases} \frac{\exp\left(43.494 - \frac{6545.8}{T+278}\right)}{(T+868)^2}, & T \leq 0\,^\circ\mathrm{C} \\ \frac{\exp\left(34.494 - \frac{4924.99}{T+237.1}\right)}{(T+105)^{1.57}}, & T > 0\,^\circ\mathrm{C} \end{cases} \tag{3}$$

Other constant properties used for air and water vapor are given in Table 4.

Table 4. Air and water vapor constant properties.

Property	Value	Unit
Water vapor's specific heat capacity, $C_{p,v}$	1872	J/(kg·K)
Water vapor gas constant, R_v	461.5	J/(kg·K)
Air gas constant, R_v	287	J/(kg·K)

3.3. Energy Calculations

Considering the whole of the air in the pipe as the control volume, the energy balance for the pipe alone becomes

$$\dot{Q} + \dot{m}(h_i - h_o) = 0 \tag{4}$$

The mass flow rate $\dot{m}$ is considered constant and calculated as follows:

$$\dot{m} = \rho_{air}(T_{av}) \cdot \pi \left(\frac{D_{in}}{2}\right)^2 \cdot U_{air} \tag{5}$$

where $\rho_{air}(T_{av})$ is the density of dry air at an average temperature, T_{av}, which is calculated by finding the average value between inlet and outlet temperatures at each timestep during the period studied and then averaging that value over time.

The enthalpy of the inlet and exit air is calculated depending on the temperature and humidity ratio as follows:

$$\begin{cases} h = h_a + \omega h_v \\ h_a = C_{p,a}(T_a) \cdot T_a \\ h_v = -0.0013 T_a^2 + 1.8834 T_a + 2501 \end{cases} \tag{6}$$

where air is considered an ideal gas when calculating h_a; however, the h_v formula was obtained by curve fitting to data available in a book by Moran et al. [20].

To convert the measurements of relative humidity to the humidity ratio, which is needed in the equation, the following formula was used:

$$\omega = \frac{0.622}{\frac{P}{RH \cdot P_{sat}(T_a)} - 1} \tag{7}$$

where P and RH are the pressure and relative humidity, respectively, measured at a specific location and time.

3.4. Exergy Calculations

The general exergy equation states that the net exergy rate transfer by heat, work, and mass, balances the net rate of exergy destroyed in the system:

$$\dot{E}x_i - \dot{E}x_o = \dot{E}x_{d,EAHE} \tag{8}$$

Considering the same control volume as for the energy equation, (8) becomes

$$\dot{E}x_{heat} + \dot{E}x_{work} + \dot{E}x_{mass,i} - \dot{E}x_{mass,o} = \dot{E}x_{d,EAHE} \tag{9}$$

Substituting each exergy term by its corresponding formula, (9) becomes

$$\left(1 - \frac{T_0}{T_w}\right)\dot{Q} + \dot{W}_{mec} + \dot{m}\psi_i - \dot{m}\psi_o = \dot{E}x_{d,EAHE} \tag{10}$$

where T_0 is the reference temperature, which is the temperature of the environment chosen, and T_w is the tube wall temperature, which is calculated as a function average of the three wall temperature measurements recorded along the tube. Noting that in other studies, this wall temperature T_w was either just measured at one point [14] or calculated relying on the constant temperature of undisturbed soil [11].

The mechanical power delivered by the fan to the air is defined by

$$\dot{W}_{mec} = \dot{W}_{electric} \cdot \eta_{fan} \tag{11}$$

ψ_i and ψ_o are the specific flow exergies, which are determined using the humid air flow exergy formulated by Dincer and Sahin [21]:

$$\begin{aligned}\psi_n = {} & (C_{p,a} + \omega_n \cdot C_{p,v})(T_n - T_0) - T_0 \cdot (C_{p,a} + \omega_n \cdot C_{p,v}) \cdot \ln\left(\frac{T_n}{T_0}\right) + T_0 \cdot (R_a + \omega_n \cdot R_v) \cdot \ln\left(\frac{P_n}{P_0}\right) \\ & + T_0 \cdot (R_a + \omega_n \cdot R_v) \cdot \ln\left(\frac{1+1.6078\omega_0}{1+1.6078\omega_n}\right) + T_0 \cdot 1.6078 \cdot \omega_n \cdot R_a \cdot \ln\left(\frac{\omega_n}{\omega_0}\right)\end{aligned} \tag{12}$$

such that n is any point along the flow and T_0, P_0, and ω_0 are the reference values of the temperature, pressure, and humidity ratios, respectively. Specific flow exergies were calculated using simpler formulas in other studies without considering the variations in pressure and humidity in the flow [8,11,12]. The same Formula (12) was used in [9,14] but without an accurate measurement of the pressure and humidity of air flow as performed in this study.

The exergy balance in Equation (10) can be applied to the different components of the system by considering the energy flows specific to each component consisting of the filter at the inlet of the system, the pipe alone, and the fan at the exit of the system, resulting in the following equations:

- Exergy balance for the filter:

$$(\dot{m}\psi_i - \dot{m}\psi_o)_{filter} = \dot{E}x_{d,filter} \tag{13}$$

- Exergy balance for the pipe:

$$\left(1 - \frac{T_0}{T_w}\right)\dot{Q} + (\dot{m}\psi_i - \dot{m}\psi_o)_{pipe} = \dot{E}x_{d,\ pipe} \tag{14}$$

- Exergy balance for the fan:

$$\dot{W}_{mec} + \left(\dot{m}\psi_i - \dot{m}\psi_o\right)_{fan} = \dot{E}x_{d,\ fan} \tag{15}$$

3.5. Restricted Dead State

Exergy is evaluated according to a reference state (dead state) which is usually the environment around the system that interacts with it but does not change its intensive properties upon this interaction. In the case of the EAHE, it is sufficient to consider a restricted dead state as the chemical interactions between the system and the environment are not considered. The restricted dead state, in this case, is the surrounding ambient air. As the temperature, pressure, and humidity of the ambient air are variable, average values of temperature and humidity ratio of the month (or two months if the period considered is in between) in which the analysis is carried out are considered as reference values (T_0, ω_0) of the restricted dead state. The reference pressure (P_0) was taken as the standard sea-level atmospheric pressure of 101,325 Pa. The restricted dead state was similarly defined in other studies ([11,22]).

3.6. Performance Assessment

3.6.1. Energetic Assessment

According to energy analyses of the system, the performance can be assessed by determining the Coefficient Of Performance (*COP*), which is the heat gained/lost by the system divided by the total consumed power. Depending on the season, the system could be working in heating or cooling modes, so $\dot{Q}$ is taken as an absolute value.

$$COP = \frac{\left|\dot{Q}\right|}{\dot{W}_{mec}} \tag{16}$$

3.6.2. Exergetic Assessment

In reality, all energy systems cannot reach an efficiency of 100% due to the second law of thermodynamics that invokes the loss of some of the energy due to the irreversibility of the system processes. Conventional energy efficiency does not consider the capabilities of the system where the system cannot exceed Carnot's efficiency. A better assessment of the system is determined using the exergetic efficiency, which shows the performance of the system according to its capabilities. The exergetic efficiency of the whole EAHE system is given by

$$\eta_{ex} = \frac{\dot{E}x_o}{\dot{E}x_i} = 1 - \frac{\dot{E}x_d}{\dot{E}x_i} \tag{17}$$

$\dot{E}x_d$ is calculated from (10), and $\dot{E}x_i$ is dependent on the situation, where it includes $\dot{E}x_{mass,i}$ in all situations, $\dot{E}x_{heat}$ only in the heating case, and $\dot{W}_{mec}$ if the fan acts on the control volume. Substituting $\dot{E}x_d$ and $\dot{E}x_i$ in Equation (17) results in each situation the following equations:

- Exergetic efficiency of the whole system in heating mode:

$$\eta_{ex}^{EAHE} = 1 - \frac{\dot{E}x_d}{\dot{E}x_{mass,i} + \dot{E}x_{heat} + \dot{W}_{mec}} \tag{18}$$

- Exergetic efficiency of the filter:

$$\eta_{ex}^{filter} = 1 - \frac{\dot{E}x_{d,filter}}{\dot{E}x_{mass,i}} \tag{19}$$

- Exergetic efficiency of the pipe:

$$\eta_{ex}^{pipe} = 1 - \frac{\dot{E}x_{d,pipe}}{\dot{E}x_{mass,i} + \dot{E}x_{heat}} \tag{20}$$

- Exergetic efficiency of the fan:

$$\eta_{ex}^{fan} = 1 - \frac{\dot{E}x_{d,fan}}{\dot{E}x_{mass,i} + \dot{W}_{mec}} \tag{21}$$

4. Results and Discussion

4.1. Analysis Period

From the database of the recorded humidity and temperature measurements in the system, the measurements of the year 2018 are chosen for the analyses. Figure 3 shows the temperature measured at the inlet and outlet of the pipe during the heating period in the coldest week of 2018 (25 February to 3 March). The graph shows how the air is heated inside the pipe where it shows the temperature increase between the inlet and the outlet where the difference reached around 8 °C on some days. The variation in the inlet and outlet temperatures also shows how the EAHE stabilizes air temperature variations which is strongly required when heating a building. The outlet air temperature exceeds the value of the wall temperature at some times (e.g., on 03/2 00:00) because the wall temperature value is an average of three measured values along the pipe, as explained in Section 3.4.

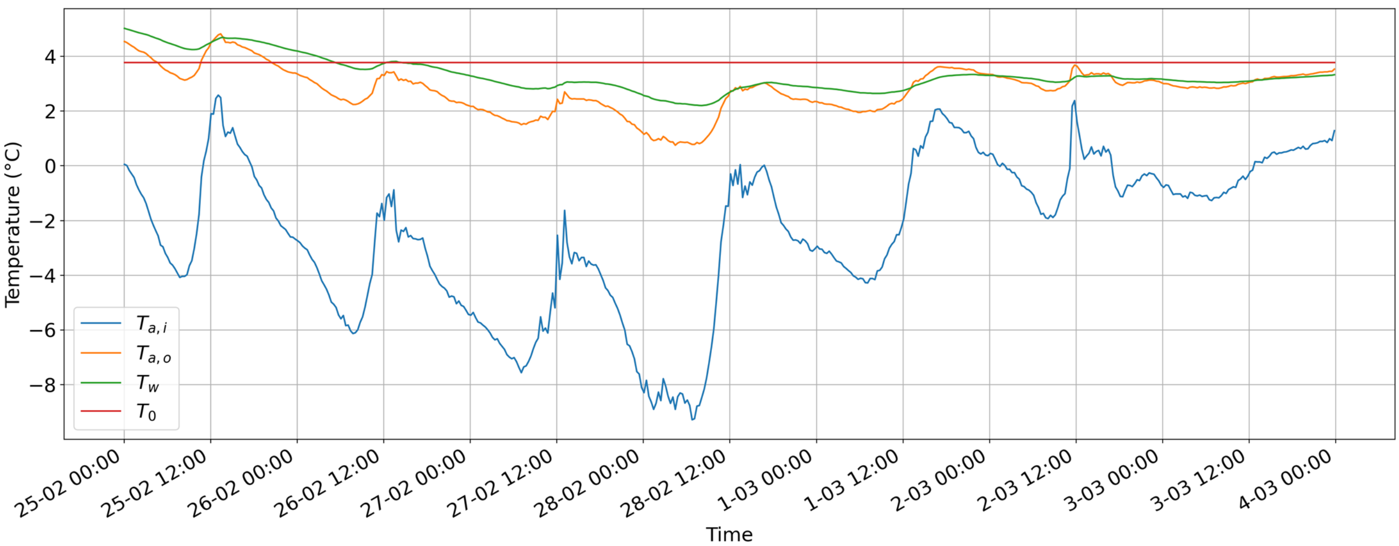

Figure 3. Measured temperatures (°C) at the inlet and outlet of the pipe compared to the estimated reference temperature during the coldest week of 2018 (25 February to 3 March).

4.2. Transferred Heat

The heat transfer calculated using Equation (4) is shown in Figure 4. This figure shows the variation in heat gained by the air as it passes through the pipe. The value increases each day during the night until it reaches a maximum in the early morning and then starts to decrease as ambient air temperature increases during the day. Obviously, the heat rate, $\dot{Q}$, is higher when the inlet air temperature is lower, as that increases the temperature difference between inlet and outlet air flows. During the chosen week, the maximum value is about 735 W reached on 28 February, while the minimum is about 67 W reached on 2 March. In total, the EAHE provided about 63 kWh of heat energy during the studied period.

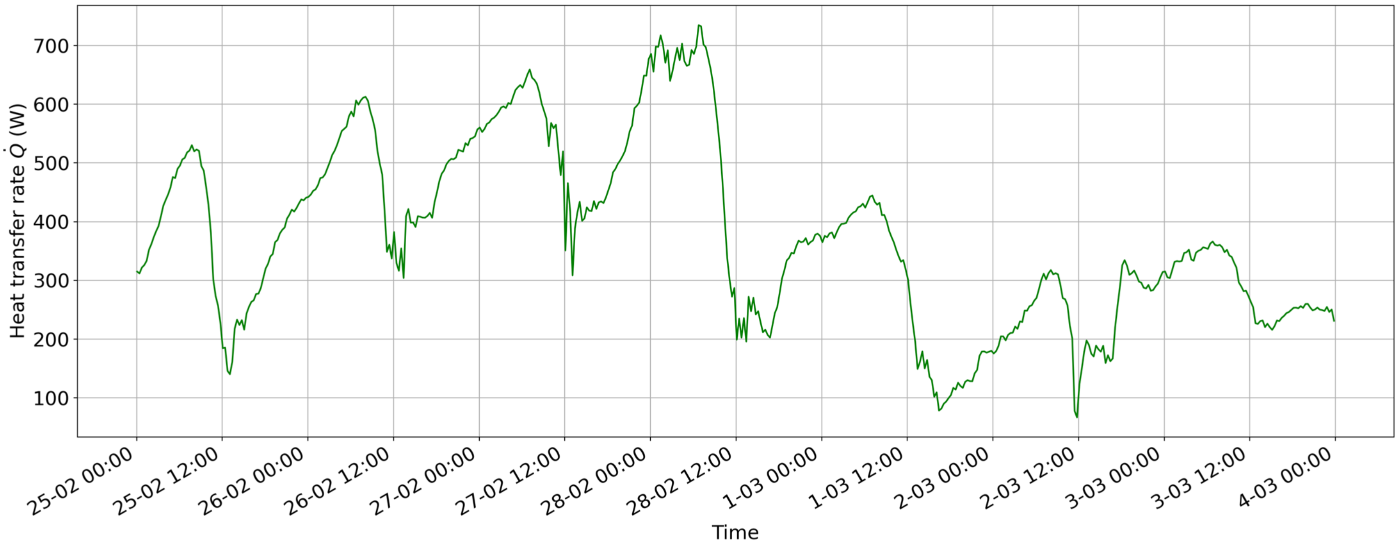

Figure 4. Heat transfer rate gained by the air as passing in the pipe in between the filter and the pipe during the analysis period.

4.3. Exergy Rates

Figure 5 shows the variation in exergy rates entering and exiting the whole EAHE system. The specific exergy rates are multiplied by the mass flow rate to obtain the mass flow exergy values shown in the figure. Despite the increase in air temperature as it crosses the pipe, the exergy of the mass flow at the exit is lower than that at the inlet. This is because the difference between the reference temperature T_0 and the inlet air temperature is higher than the difference with the outlet air temperature. As explained, T_0 was calculated as the average ambient temperature for February and March. The graph also shows the exergy of heat transfer which is relatively low because the boundary temperature (wall temperature, T_w) is so close to the reference temperature T_0. The heat transfer exergy decreases beyond zero and becomes negative when the boundary temperature is lower than the reference temperature, and this happened after 26 February. The exergy of the work of the fan is not related to temperature and is the same as the value of that work, so it is constant at $\dot{W}_{mec} = 31.2$ W all the time.

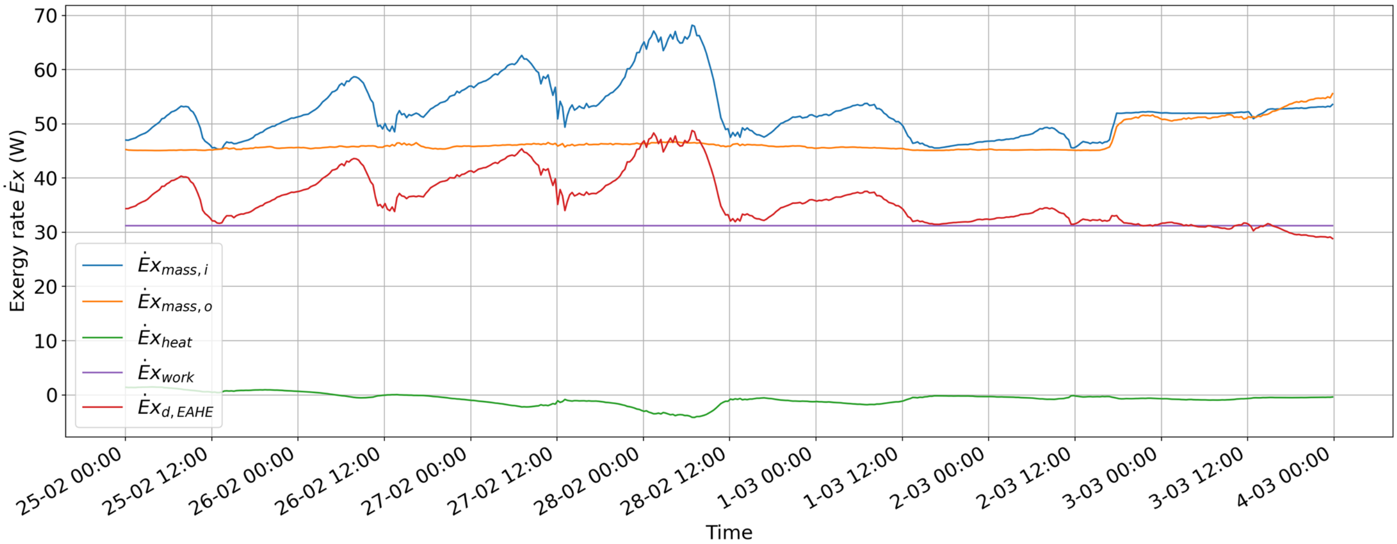

Figure 5. Exergy rates transferred to or from the system during the analysis period.

The destroyed exergy in each component of the system is shown in Figure 6. The figure shows the share of exergy destruction between the filter, pipe, and fan of the EAHE. Obviously, most of the exergy is being destroyed at the level of the fan, and the lowest destruction is at the level of the filter. Exergy destruction in the filter and the fan is almost constant because it is mainly dependent on the pressure difference between the inlet and outlet of each component which was assumed to be constant. There is slightly more variation in the exergy destruction in the filter because it is also affected by the humidity ratio, which was measured in the ambient atmosphere and after the filter, because the filter could trap some of that water content. Exergy destruction inside the pipe is what varies the most due to its dependence on exergy exchanged by the mass flow, which is mainly related to the temperature variations between the inlet and outlet of the pipe. When the inlet mass flow exergy increases, the exergy difference between inlet and outlet mass flows increases. This happens without a significant increase in the exergy rate of heat transfer due to a low boundary temperature difference with the reference temperature, as explained before. This results in an increase in the total exergy destruction rate in the system, which can be mainly seen between 25 and 28 February.

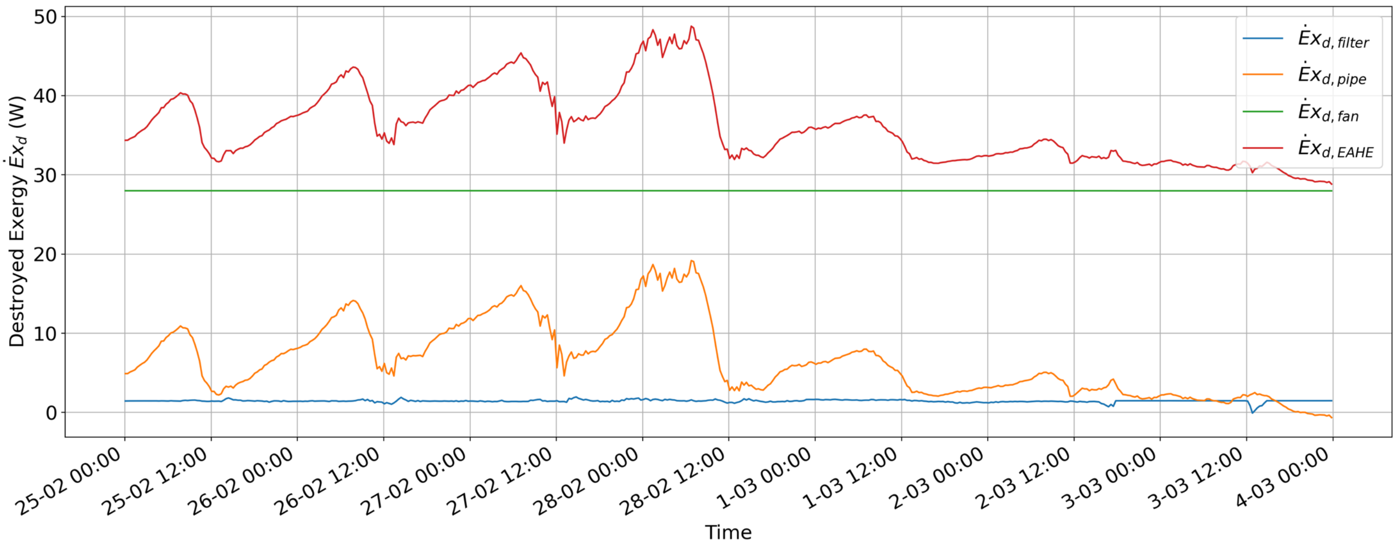

Figure 6. Exergy destroyed in each component of the system during the analysis period.

4.4. Exergetic Efficiency in Different Components

Exergetic efficiency is calculated depending on the exergy destruction in the system and could be calculated for each component alone. The variation in exergetic efficiency in each component of the EAHE is shown in Figure 7. The graph shows an opposite picture of what was seen in the graph of exergetic destruction in each component (Figure 6). The component with higher exergy destruction has lower exergetic efficiency, which is the fan that resulted in lower exergetic efficiency of the whole EAHE system. Obviously, the exergetic efficiency of the whole system is not directly the sum of the efficiencies of the components, which is the case for exergy destruction.

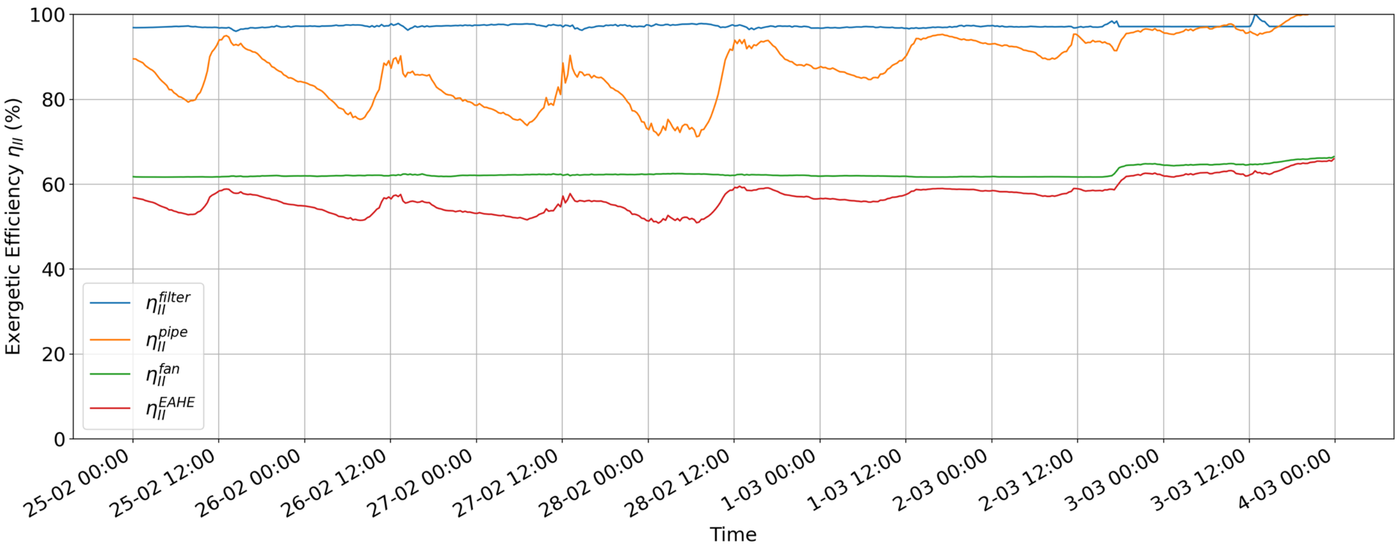

Figure 7. Exergetic efficiency variation in each component of the system during the studied period.

4.5. COP and Exergetic Efficiency

The Coefficient Of Performance (*COP*) of the system varies depending on the heat transfer rate variation, which changes with ambient temperature. Figure 8 shows this variation where *COP* reaches a maximum value of about 23.5, which coincides with the lowest inlet temperature (highest inlet-outlet temperature difference) recorded on 28 February in the morning. The minimum value of *COP* is about 2, reached when the inlet and outlet measured temperatures are the closest on 2 March at noon. In general, *COP* increases during the night and reaches its maximum in the early morning as the ambient temperature sharply decreases compared to soil temperature, which barely changes during this duration. The opposite happens when the *COP* decreases and reaches its minimum during the rest of the day. *COP* variation is higher when day-night ambient temperature variation is higher.

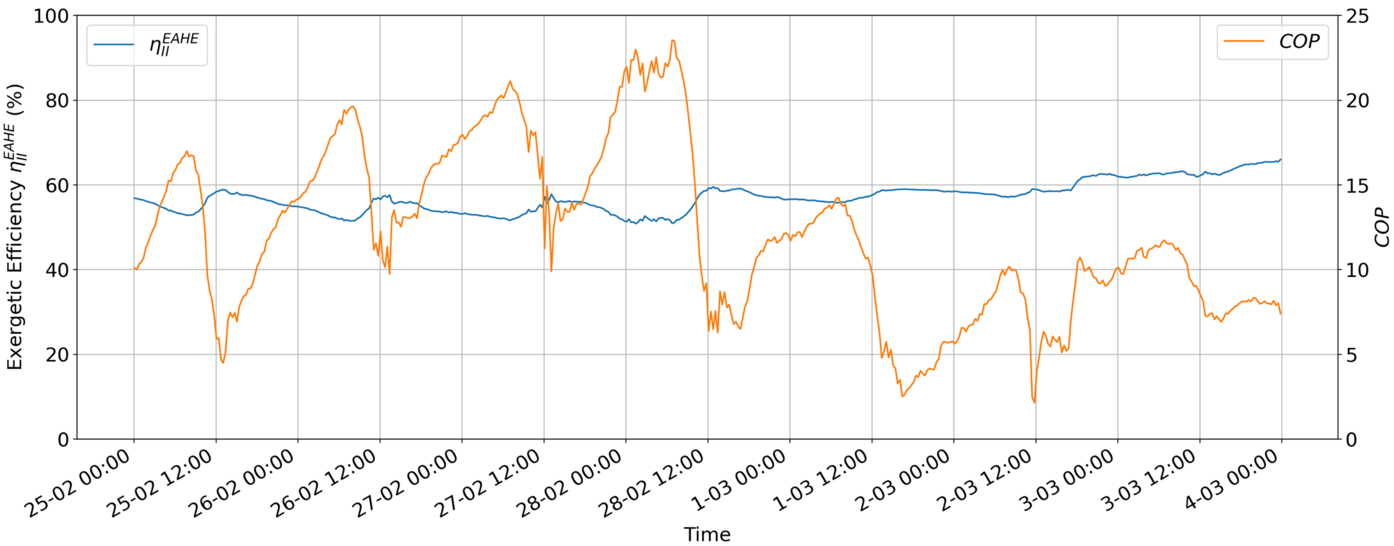

Figure 8. Performance assessment of the EAHE showing the variation in the *COP* and the exergetic efficiency of the system during the coldest week of 2018.

Figure 8 also shows the variation in the exergetic efficiency, which was formulated in Equation (18). The variation in exergetic efficiency is lower because it is more related to the variation in the inlet mass flow exergy and the destroyed exergy, which in term are both strongly related and thus compensate for one another resulting in a more stable outcome. The exergetic efficiency varies between around 50% and 66%, which is about 57% on average. Opposite to *COP*, the exergetic efficiency decreases when the inlet temperature decreases because that is when the exergetic destruction and exergy of mass flow increase. This behavior is explained by Equation (18).

5. Conclusions

Energetic and exergetic analyses were performed on an experimental EAHE site in the northeast of France to determine the efficiency of the system from both perceptions. The calculations were performed using pressure, humidity, and temperature measurements and considering variable control volume boundary temperature when calculating the exergy of heat transfer. The energetic and exergetic performance of the whole system and different components have been assessed by the calculation of *COP* and exergetic efficiency.

The analyses were carried out during a heating period in 2018. Results showed that the heat energy gained using the system was around 63 kWh using around 6.5 kWh of electricity during the analysis period.

The *COP* of the system depends mainly on the outside air temperature. Its variation is consequently very important: from about 2 to 23.5. This energetic analysis confirmed that the system could decrease the heating expenses using free geothermal energy by pre-heating the air supplied to a building.

On the other hand, despite a low heat transfer exergy due to little difference between boundary and reference temperatures, the total exergetic efficiency of the whole EAHE system is quite stable all along the analysis period. It varies between around 50% and 66%, with an average of about 57%.

By exergy destruction of different components, it was found that exergy is mostly destroyed in the fan while the lowest destruction was in the filter. This resulted in lower exegetic efficiency in the fan than in other components. Therefore, the fan should mainly be improved to lower the exergy destruction in the system and thus increase the efficiency of the whole system.

Moreover, the exergy analysis showed that exergy is strongly related to the environment where the variations in temperature, humidity, and pressure of air in the ambient environment strongly affect the values of heat and flow exergies and, thus, exergy destruction and exergetic efficiency. Therefore, the system's performance is dependent on the weather in the location where it is being used, and its profitability should be studied carefully in each location.

Author Contributions: Conceptualization, W.Z. and M.S.; methodology, W.Z.; software, W.Z.; validation, W.Z., J.L. and M.S.; formal analysis, W.Z.; investigation, W.Z. and J.L.; resources, J.L.; data curation, J.L.; writing—original draft preparation, W.Z.; writing—review and editing, J.L. and M.S.; visualization, W.Z.; supervision, M.S.; project administration, M.S.; funding acquisition, M.S. All authors have read and agreed to the published version of the manuscript.

Funding: This research received no external funding.

Data Availability Statement: Not applicable.

Conflicts of Interest: The authors declare no conflict of interest.

Nomenclature

Cp	specific heat capacity $\left(\frac{\text{J}}{\text{kgK}}\right)$
COP	Coefficient Of Performance
D	diameter (m)
$\dot{E}x$	Exergy (W)
h	specific enthalpy $\left(\frac{\text{J}}{\text{kg}}\right)$
L	length (m)
$\dot{m}$	mass flow rate $\left(\frac{\text{kg}}{\text{s}}\right)$
P	pressure (Pa)
$\dot{Q}$	heat transfer rate (W)
R	gas constant $\left(\frac{\text{J}}{\text{kgK}}\right)$
RH	relative humidity
T	temperature (K)
U	velocity $\left(\frac{\text{m}}{\text{s}}\right)$
$\dot{W}$	work (W)
η	efficiency
λ	thermal conductivity $\left(\frac{\text{J}}{\text{mK}}\right)$
ρ	density $\left(\frac{\text{kg}}{\text{m}^3}\right)$
ψ	specific flow exergy $\left(\frac{\text{W}}{\text{kg}}\right)$
ω	humidity ratio $\left(\frac{\text{kg}_{\text{vapor}}}{\text{kg}_{\text{dry air}}}\right)$
Subscripts	
a	air
av	average
d	destroyed
ex	exergetic
in	inner
i	inlet
mec	mechanical
n	referring to any location
o	outlet
sat	saturation
tot	total
v	vapor
w	wall
0	reference value

References

1. International Energy Agency. *Transition to Sustainable Buildings*; IEA: Paris, France, 2013.
2. Enerdata. Evolution of Households Energy Consumption Patterns across the EU. Available online: https://www.enerdata.net/publications/executive-briefing/households-energy-efficiency.html (accessed on 13 December 2022).
3. International Energy Agency. *The Future of Cooling*; IEA: Paris, France, 2018.
4. British Petroleum bp. Statistical Review of World Energy 2021; 2021; Volume 70. Available online: https://www.bp.com/content/dam/bp/business-sites/en/global/corporate/pdfs/energy-economics/statistical-review/bp-stats-review-2021-full-report.pdf (accessed on 13 December 2022).
5. European Commission, Heating and Cooling. Available online: https://energy.ec.europa.eu/topics/energy-efficiency/heating-and-cooling_en (accessed on 13 December 2022).
6. Márquez, J.A.; Bohórquez, M.M.; Melgar, S.G. Ground Thermal Diffusivity Calculation by Direct Soil Temperature Measurement. Application to very Low Enthalpy Geothermal Energy Systems. *Sensors* **2016**, *16*, 306. [CrossRef] [PubMed]
7. Moran, M.J.; Sciubba, E. Exergy Analysis: Principles and Practice. *J. Eng. Gas Turbines Power* **1994**, *116*, 285–290. [CrossRef]
8. Esen, H.; Inalli, M.; Esen, M.; Pihtili, K. Energy and exergy analysis of a ground-coupled heat pump system with two horizontal ground heat exchangers. *Build. Environ.* **2007**, *42*, 3606–3615. [CrossRef]
9. Yildiz, A.; Ozgener, O.; Ozgener, L. Exergetic performance assessment of solar photovoltaic cell (PV) assisted earth to air heat exchanger (EAHE) system for solar greenhouse cooling. *Energy Build.* **2011**, *43*, 3154–3160. [CrossRef]

10. Hepbasli, A. Low exergy modelling and performance analysis of greenhouses coupled to closed earth-to-air heat exchangers (EAHEs). *Energy Build.* **2013**, *64*, 224–230. [CrossRef]
11. Misra, R.; Jakhar, S.; Agrawal, K.K.; Sharma, S.; Jamuwa, D.K.; Soni, M.S.; Agrawal, G.D. Field investigations to determine the thermal performance of earth air tunnel heat exchanger with dry and wet soil: Energy and exergetic analysis. *Energy Build.* **2018**, *171*, 107–115. [CrossRef]
12. Afrand, M.; Shahsavar, A.; Sardari, P.T.; Sopian, K.; Salehipour, H. Energy and exergy analysis of two novel hybrid solar photovoltaic geothermal energy systems incorporating a building integrated photovoltaic thermal system and an earth air heat exchanger system. *Sol. Energy* **2019**, *188*, 83–95. [CrossRef]
13. Ozgener, L.; Ozgener, O. An experimental study of the exergetic performance of an underground air tunnel system for greenhouse cooling. *Renew. Energy* **2010**, *35*, 2804–2811. [CrossRef]
14. Ozgener, O.; Ozgener, L. Exergetic assessment of EAHEs for building heating in Turkey: A greenhouse case study. *Energy Policy* **2010**, *38*, 5141–5150. [CrossRef]
15. Cuny, M.; Lin, J.; Siroux, M.; Magnenet, V.; Fond, C. Influence of coating soil types on the energy of earth-air heat exchanger. *Energy Build.* **2018**, *158*, 1000–1012. [CrossRef]
16. Cuny, M.; Lin, J.; Siroux, M.; Fond, C. Influence of an improved surrounding soil on the energy performance and the design length of earth-air heat exchanger. *Appl. Therm. Eng.* **2019**, *162*, 114320. [CrossRef]
17. Cuny, M.; Lin, J.; Siroux, M.; Fond, C. Influence of rainfall events on the energy performance of an earth-air heat exchanger embedded in a multilayered soil. *Renew. Energy* **2020**, *147*, 2664–2675. [CrossRef]
18. Zografos, A.I.; Martin, W.A.; Sunderland, J.E. Equations of properties as a function of temperature for seven fluids. *Comput. Methods Appl. Mech. Eng.* **1987**, *61*, 177–187. [CrossRef]
19. Huang, J. A Simple Accurate Formula for Calculating Saturation Vapor Pressure of Water and Ice. *J. Appl. Meteorol. Climatol.* **2018**, *57*, 1265–1272. [CrossRef]
20. Moran, M.J.; Shapiro, H.N.; Boettner, D.D.; Bailey, M.B. *Fundamentals of Engineering Thermodynamics*, 8th ed.; Wiley: Hoboken, NJ, USA, 2014.
21. Dincer, I.; Sahin, A.Z. A new model for thermodynamic analysis of a drying process. *Int. J. Heat Mass Transf.* **2004**, *47*, 645–652. [CrossRef]
22. Kallio, S.; Siroux, M. Energy Analysis and Exergy Optimization of Photovoltaic-Thermal Collector. *Energies* **2020**, *13*, 5106. [CrossRef]

Disclaimer/Publisher's Note: The statements, opinions and data contained in all publications are solely those of the individual author(s) and contributor(s) and not of MDPI and/or the editor(s). MDPI and/or the editor(s) disclaim responsibility for any injury to people or property resulting from any ideas, methods, instructions or products referred to in the content.